coatings

MDPI

Article

High Absorptivity and Ultra-Wideband Solar Absorber Based on Ti-Al_2O_3 Cross Elliptical Disk Arrays

Yuanjian Zhang [1,†], Yingting Yi [2,†], Wenxin Li [1], Shiri Liang [1], Jing Ma [1], Shubo Cheng [1,*], Wenxing Yang [1,*] and Yougen Yi [2,*]

[1] School of Physics and Optoelectronic Engineering, Yangtze University, Jingzhou 434023, China
[2] College of Physics and Electronics, Central South University, Changsha 410083, China
* Correspondence: shubocheng@yangtzeu.edu.cn (S.C.); wenxingyang2@126.com (W.Y.); yougenyi@csu.edu.cn (Y.Y.)
† These authors contributed equally to this work and should be considered co-first authors.

Abstract: Perfect metamaterial absorbers have attracted researchers' attention in solar energy harvesting and utilization. An ideal solar absorber should provide high absorption, be ultra-wideband, and be insensitive to polarization and incident angles, which brings challenges to research. In this paper, we proposed and optimized an ultra-wideband solar absorber based on Ti-Al_2O_3 cross elliptical disk arrays to obtain the ultra-wideband absorption of solar energy. The addition of a cavity greatly improves the energy-absorbing effect in the operating band, which has research value. The absorption spectrum and field distribution were analyzed by the finite difference time domain method. For the physical mechanism, the electric and magnetic field distribution indicates that ultra-wideband absorption is caused by propagation surface plasmon resonance (SPR), localized SPR and Fabry–Perot (F-P) resonance excited between Ti and Al_2O_3 disks. The results demonstrate that the absorption bandwidth with the absorption rate beyond 90% reaches 1380 nm (385–1765 nm), and the average absorption reaches an astonishing 98.78%. The absorption bandwidth matches the main radiation bandwidth of the solar energy, which is approximately 295–2500 nm according to the data from the literature, and the total thickness of the structure is only 445 nm. Moreover, the ultra-wideband solar absorber is insensitive to the polarization angle and oblique incidence angle. The proposed ultra-wideband solar absorber has research and application value in solar energy harvesting, photothermal conversion and utilization.

Keywords: ultra-wideband solar materials; solar energy; surface plasmon resonance; metamaterials; broadband absorbers; ultra-thin absorber

check for updates

Citation: Zhang, Y.; Yi, Y.; Li, W.; Liang, S.; Ma, J.; Cheng, S.; Yang, W.; Yi, Y. High Absorptivity and Ultra-Wideband Solar Absorber Based on Ti-Al_2O_3 Cross Elliptical Disk Arrays. *Coatings* **2023**, *13*, 531. https://doi.org/10.3390/coatings13030531

Academic Editor: Alessandro Latini

Received: 12 January 2023
Revised: 20 February 2023
Accepted: 24 February 2023
Published: 28 February 2023

Copyright: © 2023 by the authors. Licensee MDPI, Basel, Switzerland. This article is an open access article distributed under the terms and conditions of the Creative Commons Attribution (CC BY) license (https://creativecommons.org/licenses/by/4.0/).

1. Introduction

With the long-term use of non-renewable fossil energy, the impact on the environment has become increasingly prominent, and research on clean energy is an important issue today. The clean and resource-rich solar energy is the current hot direction of energy research [1,2]. Metamaterials are artificially fabricated subwavelength nanostructures, with a strong ability to manipulate electromagnetic waves [3]. Solar energy is concentrated in the visible to the near-infrared bands; metamaterial absorbers can achieve perfect absorption in the range, which is of wide concern [4].

In recent years, solar absorbers have attracted widespread attention as a pivotal device to achieve solar energy harvest [5,6]. In addition to high absorption absorptivity, an ideal absorber needs to possess other optical characteristics such as polarization independence and tunability [7,8], etc. Nevertheless, current absorbers are generally temperature sensitive, light absorption inefficient and complex [9,10]. Consequently, how to solve these problems determines the current development direction of solar absorbers.

The research on wideband absorbers has continued for many years [11–15] since Landy et al. first proposed the perfect material based on a metal–insulator–metal structure

in 2008 [16]. Absorbers based on this structure have been widely investigated. Among them, wideband absorbers that can achieve perfect broadband absorption have great application potential in photovoltaics and solar cells [17,18]. The special material properties of noble metals such as gold and silver have made them widely used for perfect absorption previously [19,20]. However, the high cost and poor heat resistance also limited the application potential of materials composed with noble metal; thus, people started to consider the high melting point metals such as titanium, nickel, tungsten and others [21,22]. There are several common ways to achieve wideband absorption at present. For instance, Hu et al. placed multiple different nanoresonators in a unit cell. These different resonators can excite multiple absorption peaks in the spectrum. In this way, the wideband absorption can be achieved. The disadvantage is that the structure is complex and is difficult to manufacture [23]. Cui et al. proposed a thin-film stacked structure formed by stacking metal–dielectric layers to realize a wide-spectrum material [24]. This kind of material achieves wideband absorption in the mid-infrared band and are insensitive to the incident angle, and the thickness is very thin (thickness < 190 nm). Although the proposals of these materials have provided ideas for subsequent research, broadband absorbers for solar energy harvesting not only need to match the bandwidth to the solar radiation spectrum mainly distributed at 295–2500 nm under the AM1.5 [25] but also meet the highest absorption rate. Therefore, how to improve the absorption rate in the solar radiation spectrum is the focus of this paper.

In this paper, we studied the absorber based on Ti-Al_2O_3 cross elliptical disk arrays. We added a layer of dielectric on top of the traditional MIM structure for anti-reflection purposes and to achieve better absorptivity. In order to make the overall arrays have good thermal stability and high absorptivity, we used two materials, metal titanium and dielectric Al_2O_3. The inherent optical properties of the materials and excellent structure achieved over 90% ultra-wideband absorption at the wavelength from 385 nm to 1765 nm, verified by simulation. The arrays we designed more than achieved ultra-wideband absorption and matched well with the solar energy spectrum. The proposed absorber can obtain a perfect absorption performance in the actual solar radiation environment, and has potential applications on solar energy harvesting and shielding.

2. Structure and Design

Figure 1 details the proposed ultra-wideband solar material. The total four-layer structure is composed of two materials: Ti and Al_2O_3. There is a three-layer cross elliptical disk array on the Ti substrate periodically, there are cross elliptical disks made of Al_2O_3 inserted to cover the structure, and the middle layer is a metal Ti cross elliptical disk with a cavity in the middle. The period of the cross elliptical disks is represented by P. The radius of the major axis of the ellipse is R, the minor axis is r and a is the radius of the cavity in Ti cross elliptical disks. h_1, h_2 and h_3 are the thicknesses of the cross elliptical disks that made by Al_2O_3 and Ti from top to bottom, respectively. The metal Ti substrate needs to be thick enough to reduce the light transmittance of arrays to almost zero. Electron beam lithography [26] and vapor deposition technology [27] can be used to realize the manufacturing of this structure. The cost of the materials we selected is not high, but limited to the current process, the preparation cost is very high, and the error is difficult to control. With the progress of technology, the cost will reduce. Simulation research can carry out prospective study at low cost. Many of the ideas similar to that which Landy proposed in 2008 by simulation research [16] are creative and progressive, enlightening researchers and greatly saving their costs. Due to the high cost of the experiment and insufficient experimental conditions, our current research mainly focuses on theoretical simulation. If the experimental conditions are sufficient, we will fabricate the proposed pattern array on 1 mm^2 substrate material [28].

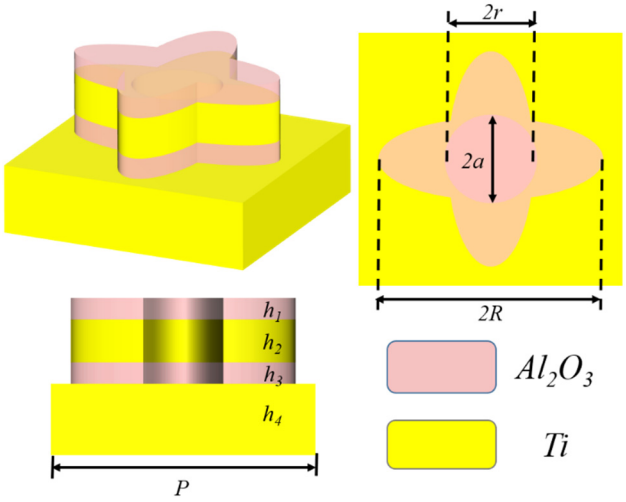

Figure 1. Diagram of titanium and Al_2O_3 elliptical disk cross-structure of broadband absorber.

The finite difference time domain method is used in the simulation with 3D FDTD solutions software [29,30]. By applying periodic boundary conditions in the x and y directions, the entire arrays can be simplified to a unit cell. The transverse magnetic mode (TM, x-axis polarization) plane waves are incident vertically from above the arrays, and the transmission and reflection effects are truncated by perfect matched layer boundary in the z direction, and all three directions of mesh are set to 2.5 nm. TM mode and transverse electric (TE) mode here is the x-axis polarization or y-axis polarization of the incident light, respectively. The detailed parameters of the proposed absorber in the simulation are taken as P = 400 nm, R = 170 nm, r = 65 nm, a = 70 nm, h_1 = 60 nm, h_2 = 115 nm, h_3 = 70 nm and h_4 = 200 nm, and parameters for metal Ti and Al_2O_3 are taken from the experimental data of Palik [31]. In the simulation, the transmission T and reflection R of the structure can be recorded by setting the monitor. Then the total absorption A can be calculated using the formula $A = 1 - T - R$ [32–34].

3. Results and Discussion

The simulation results of the proposed absorber are shown in Figure 2. It can be seen that the proposed absorber exhibits excellent high absorptivity at the wavelength from 280 nm to 2000 nm, the bandwidth at which absorptivity reaches above 90% is 1380 nm (385–1765 nm), which matches the solar radiation range well. The average absorptivity in the wavelength band of 385 nm to 1765 nm reaches 98.78%. In the entire solar radiation region (295–2500 nm), there is still a high absorptivity of 93.7%. Among them, more than 99% high absorption is achieved at 547.7 nm, 702.2 nm and 1092.3 nm. A comparison with some recent solar absorbers is shown in Table 1 [8,35–40], the proposed absorber clearly obtained the widest absorption bandwidth.

Table 1. Comparison of some recent solar energy absorbers.

References	Spectral Region with Absorption More than 90%	Pattern	Materials
[8]	200–1000 nm (800 nm)	Alternate stacked	Au/Cr/Graphene/TMDs
[35]	300–1015 nm (715 nm)	Wavy surface	Indium tin oxide-Ge-Cu
[36]	400–850 nm (450 nm)	Cubes	Au/MoS_2
[37]	250–1100 nm (850 nm)	Disk and Nanoparticles	Au/HfO_2
[38]	287–628 nm (341 nm)	Disk	Si/Ni
[39]	380–760 nm (475 nm)	Half-cylinder air cavity	TiO_2
[40]	200–2500 nm (peak absorbance lower than 90%)	Helical	Bismuth
Proposed	385–1765 nm (1380 nm)	Cross elliptical disk	Ti/Al_2O_3

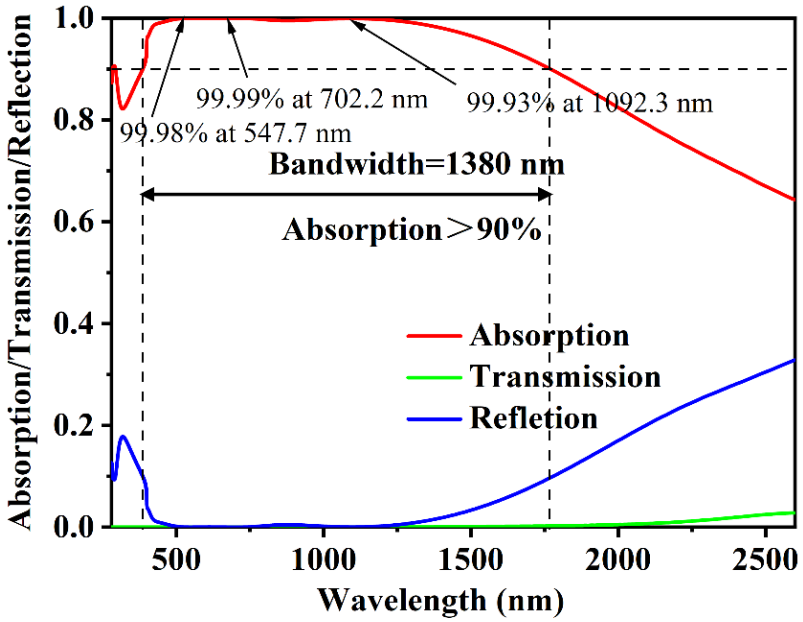

Figure 2. Absorption of cross ellipses broadband absorber.

In order to verify the utilization effect of our high absorptivity absorber on solar energy, we used the AM1.5 solar radiation spectrum to simulate the lighting conditions of the real environment, and calculated the performance of the proposed absorber in the actual situation. The calculation method of solar energy absorption efficiency is referred to in this equation [41–43]:

$$\eta_A = \frac{\int_{\lambda_{min}}^{\lambda_{max}} (1 - R(\omega)) \cdot I_{AM1.5}(\omega) \cdot d\omega}{\int_{\lambda_{min}}^{\lambda_{max}} I_{AM1.5}(\omega) \cdot d\omega} \quad (1)$$

In this equation, η_A is the absorptivity, $R(\omega)$ is the reflection of arrays, the frequency of the incident source is ω and $I_{AM1.5}$ is the sun radiation. The results are presented in Figure 3.

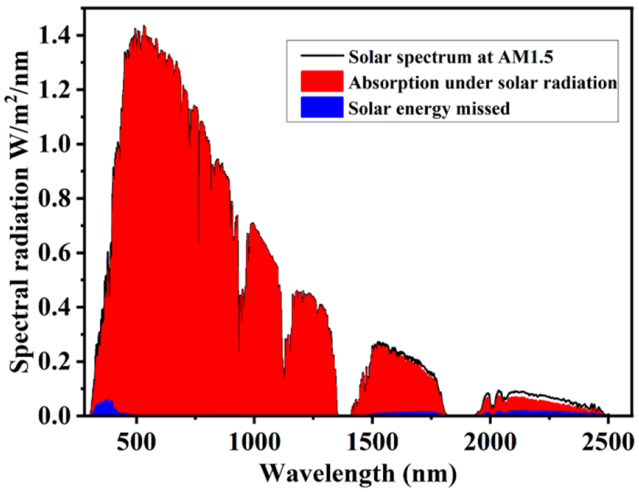

Figure 3. Absorption and unabsorbed energy under a solar spectrum at AM 1.5.

For reference, the AM1.5 solar radiation spectrum is plotted with a black curve in Figure 3. The large red area under the black curve is the solar energy that can be absorbed by the proposed absorber. It is clear that the result is very satisfactory. Most of the energy can be absorbed, and the lost energy is represented by the blue area in Figure 3. It is very

intuitive to see that its proportion is very low, and it is mainly concentrated in the two bands of 290–500 nm and 1500–2500 nm. A smaller blue area means a lower amount of energy was missed. The missed solar energy was only 1.6% at the wavelength from 280 nm to 2600 nm. This also means the global absorption effect of the proposed material is excellent and matches the solar radiation well.

Through the electromagnetic field distribution diagram, we can intuitively understand the physical mechanism of the ultra-wideband perfect absorption of the absorber, and optimize the structure according to its distribution. This method has often been used in previous studies [40–45]. We calculated the electric and magnetic field distribution to explore the physical mechanism of our solar absorber at three resonance wavelengths, 547.7 nm, 702.2 nm and 1092.3 nm, as presented in Figures 4 and 5. There are three resonances that excite the ultra-wideband absorption, which are propagation surface plasmon resonance (SPR), localized SPR and Fabry–Perot (F-P) resonance [44–46]. This simulation adopted the TM-polarized mode as the incident light. Figure 4 plots the electric and magnetic field distributions of the top views from the XOY direction, and Figure 5 presents the side views from the XOZ direction.

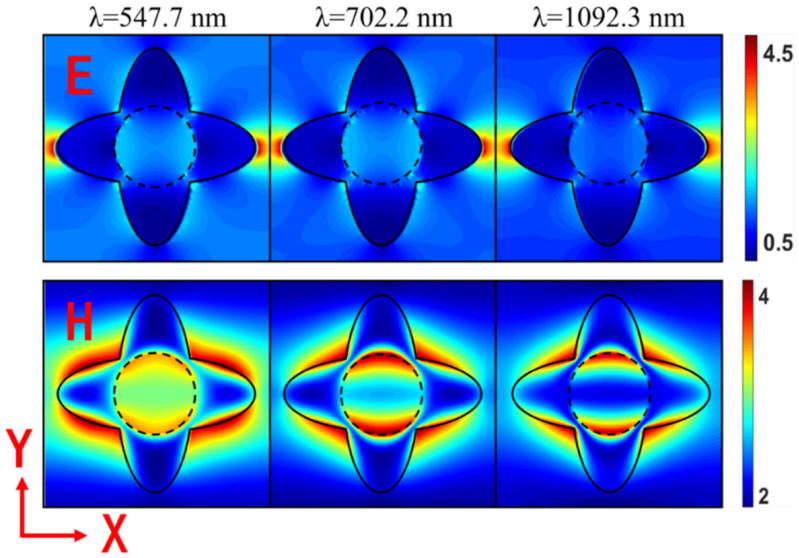

Figure 4. Electric and magnetic field distribution at three resonant wavelengths in the XOY direction.

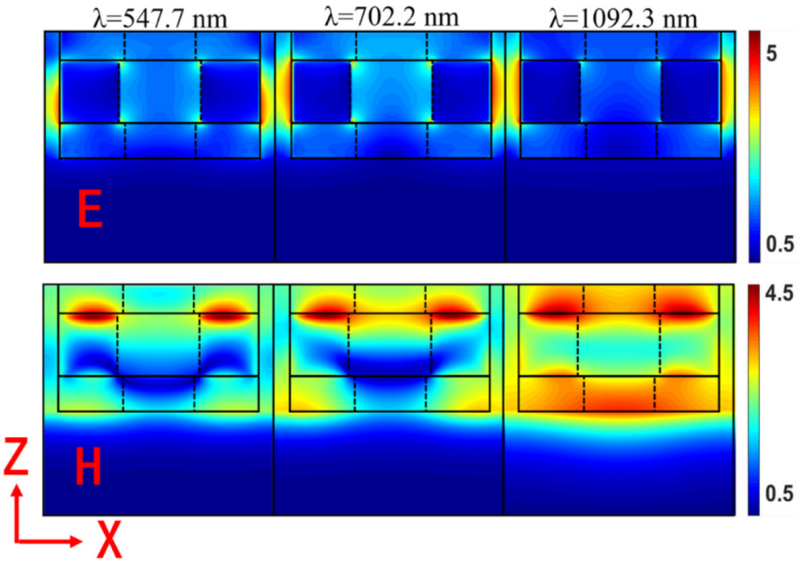

Figure 5. Electric and magnetic field distribution at three resonant wavelengths in the XOZ direction.

At the 547.7 nm resonance wavelength, the electric field is mainly concentrated in the gaps between the periodic arrays of metal Ti in the middle layer, and the magnetic field strength is mainly concentrated on the plane between the metal Ti and the Al_2O_3 on the top layer outside of the arrays. These features indicate that the absorption observed at 547.7 nm is mainly due to the propagation SPR of the Ti elliptical disk. For the case where the resonance wavelength is 702.2 nm, the electric field is still concentrated in the gaps between the periodic arrays. This means propagation SPR is excited as before, and the concentration of the magnetic field turns to the cavity inside the metal Ti and Al_2O_3 on the top layer, indicating that there is a slight coupling between the elliptical disks and localized SPR is excited, which demonstrates that the perfect absorption at the wavelength of 702.2 nm is the synergy of the propagating SPR and the localized SPR. For the wavelength of 1092.3 nm, however, the magnetic field is concentrated in the Al_2O_3 layer between the metals and the Al_2O_3 layer covering the top, as shown in Figures 4 and 5, and due to the excitation of localized SPR, it caused magnetic resonance. At this time, the middle layer Ti, substrate Ti and dielectric layer constitute the inductor–capacitor circuit [47]. The current in the middle and bottom metal layers is in a different direction, forming a loop current. Its direction is opposite to the direction of the incident electromagnetic wave, and they therefore counteract each other and this limits the electromagnetic wave in the middle dielectric layer. It means that the F-P cavity and localized SPR lead to light absorption at 1092.3 nm.

We already know that the cross elliptical disk arrays can achieve ultra-wideband high absorptivity at the previous solar radiation region. In order to achieve the best results, we also investigated different nanostructures. Firstly, we studied several different but similar structure models, and the results are plotted in Figure 6. We kept the geometrical parameters constant to compare the proposed material with different cases. For Case1, the elliptical disk structure has only one absorption peak reaching 97.5% at a short wavelength. Unfortunately, the absorptivity is only 65.1% in the solar radiation region, much less than the cross elliptical arrays (93.7%). Then, the cross arrays achieved an absorptivity of 91.1% in the whole region as the red line presents. There is an absorption peak of 98.4% redshifted to 2016 nm, but the absorption decreases a lot in the region from 750 nm to 1700 nm where there is more solar radiation. The lowest is only 82.5% at 1090 nm. It is similar to the cross arrays in that the cross elliptical disk has an absorption peak of 99.8% redshifted to 1593 nm. There is also a lower loss in the range of 750–990 nm where the lowest at 882 nm obtains absorptivity of 89%. In the whole region of solar radiation, the cross elliptical arrays reach an absorptivity of 91.8%. Compared with the proposed absorber, although the absorption performance is similar, the energy absorption varies greatly under solar radiation. Because of the addition of the cavity, the absorption is greatly improved at the wavelength from 500 nm to 1326 nm.

To further discuss the absorption performance of different structures in a real environment, we systematically investigated the absorptivity of solar energy at AM 1.5, as shown in Figure 7. For Case1, the loss of solar energy in the entire region nears 20% as we calculated. The energy missed is relatively high from 1412 nm to 2500 nm, exceeding 40%. For Case2 and Case3, although the absorption mentioned in Figure 6 obtains 91.1% and 91.8%, respectively, the energy loss at the wavelength from 500 nm to 1300 nm is not ideal. Compared with the proposed material arrays, these losses reduce the solar radiation absorptivity in the range of 7.5% and 3.9%, respectively. The addition of an air hole in the middle Ti layer forms a resonant cavity, which can bind more electromagnetic waves in the operating range from 500 nm to 1362 nm. More absorption reduces the unabsorbed energy, although the absorption peak has some blue shift. This result is undoubtedly more suitable for solar energy absorption in practical applications as Figures 3 and 7 present.

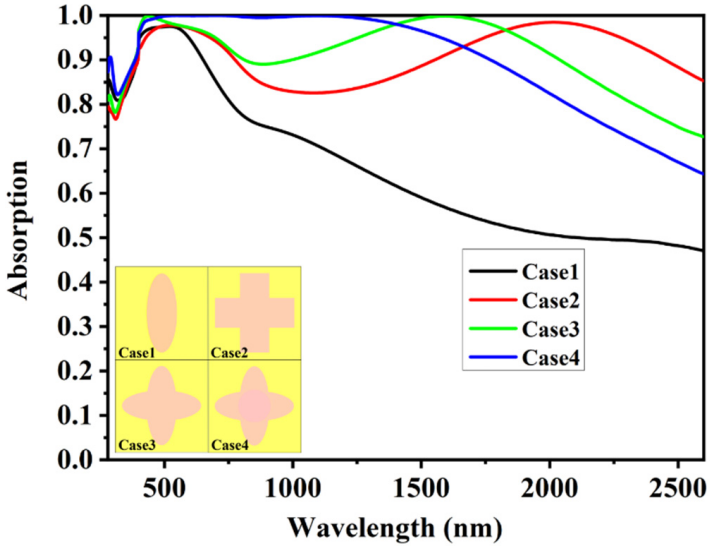

Figure 6. Absorption spectra of four different geometric structures.

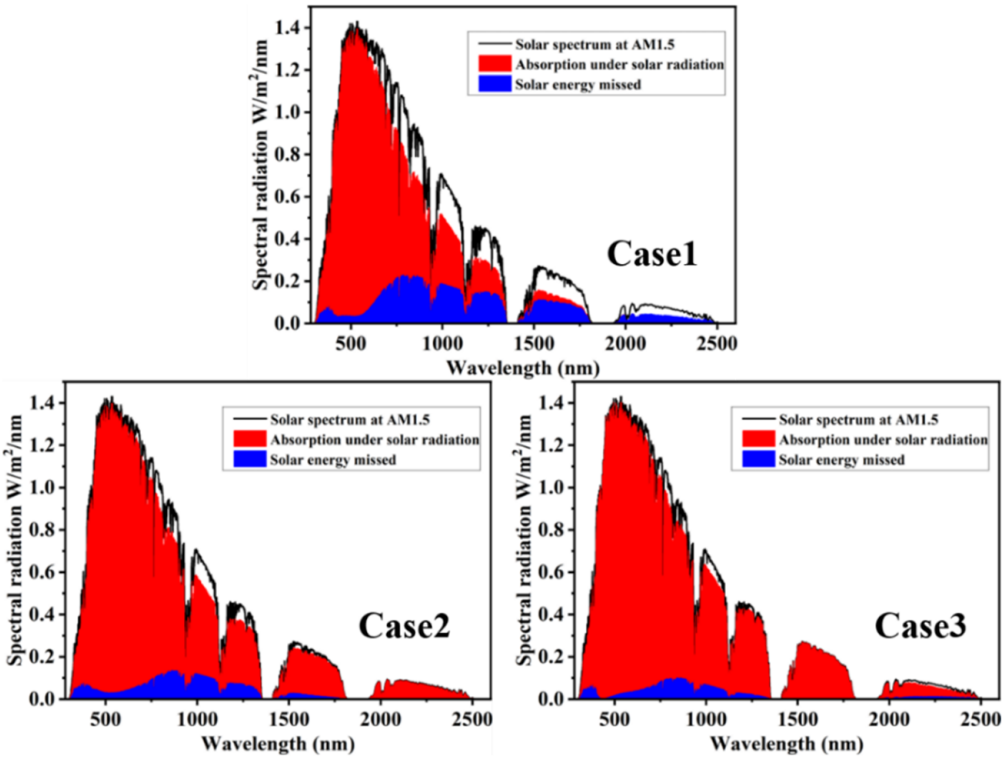

Figure 7. Solar absorption spectral for Case1 to Case3.

After that, we further investigated the influences of different stacking combinations on light absorption performance, as shown in Figure 8. The absorption when there is no Al_2O_3 layer but only a layer of Ti substrate and Ti cross elliptical disk is indicated by the black line. For Case6, the red line plots the absorptivity spectrum when there is only one Al_2O_3 layer covered by a Ti disk on top, and the green line shows only one layer of Al_2O_3 between the substrate and the Ti disk. As a contrast, the blue line is the proposed array. Clearly, when there is no Al_2O_3 layer between the substrate and the Ti disk, the arrays only achieve a narrow absorption higher than 90% from 395 nm to 800 nm, and then it drops rapidly after 800 nm. In the whole region, the absorptivity of these arrays only reaches 68.7%. The red line shows that the covered Al_2O_3 on this kind of array is less effective in improving the absorption. The absorption in the whole region increased by 1.2% to 69.9%. There is an

absorption peak of 98.8% that appeared at 292 nm, but the total absorptivity is still low. For Case7, we inserted a layer of Al_2O_3 between the substrate and Ti disk and realized an absorptivity of 89.3%, as shown by the green line. The result is close to the proposed absorber but slightly lower at the wavelength from 443 to 1190 nm. This demonstrates that the Al_2O_3 between the Ti disk and the substrate plays an important part in exciting SPR to achieve ultra-wideband absorption. Thus, a layer of Al_2O_3 covered on this basis further improves the absorption performance, as we proposed.

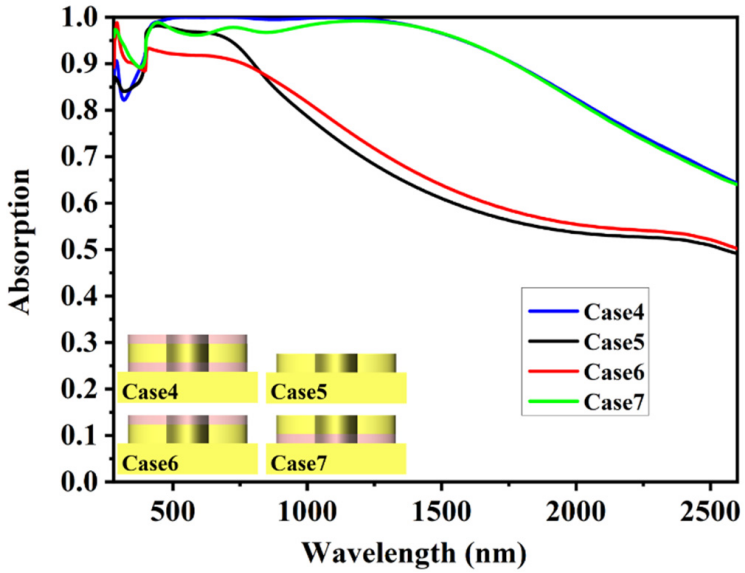

Figure 8. Absorption spectra of different layer stacking.

As in the study above, the absorptivity levels of solar radiation shown by Case5–Case7 were also investigated. From Figure 9, it is obvious that there is a high amount of energy missed over the whole region of solar radiation for Case5 and Case6. It is much higher than the 1.6% of the proposed material as the energy missed reached 12.8% and 14.1%, respectively, for Case5 and Case6. We can see that the addition of the inserted layer of Al_2O_3 greatly increases the absorptivity of solar radiation, and the high amount of energy missed is also reduced to 3.6%. However, there is still a bandwidth with a little lower absorptivity between 490 nm and 950 nm; the Al_2O_3 covering the top eliminates this loss and reduces the energy loss to 1.6%. The results of different stacking methods show that the metal and insulator in the traditional MIM structure have a huge influence on the excitation of resonances that achieve wideband absorption. While the addition of the top layer of Al_2O_3 further enhances the overall absorption effect, any part of the proposed absorber is indispensable for the total absorption performance.

We made a brief analysis of the selection of materials. The imaginary part of the dielectric constant of the metal Ti is higher in the wide wavelength band. The MIM absorber made of metal Ti can obtain high broadband absorption [48]. In addition, the metal Ti has high reserves and good heat resistance. These are the reasons why we adopted the metal Ti. For the selection of dielectric, we performed a simulation comparison as shown in Figure 10. The performance of Al_2O_3 and SiO_2 is in line with our requirements for solar absorbers, and the use of Al_2O_3 has better average absorption. It is the reason that we selected Al_2O_3 as the dielectric layer.

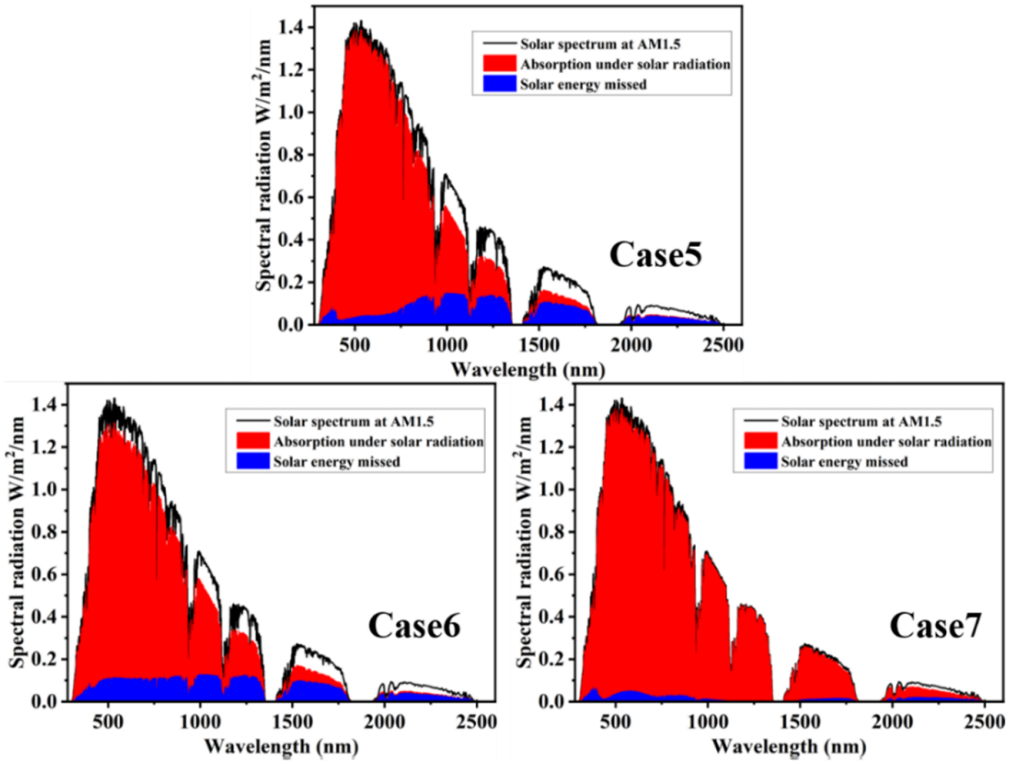

Figure 9. Solar absorption spectral for Case5 to Case7.

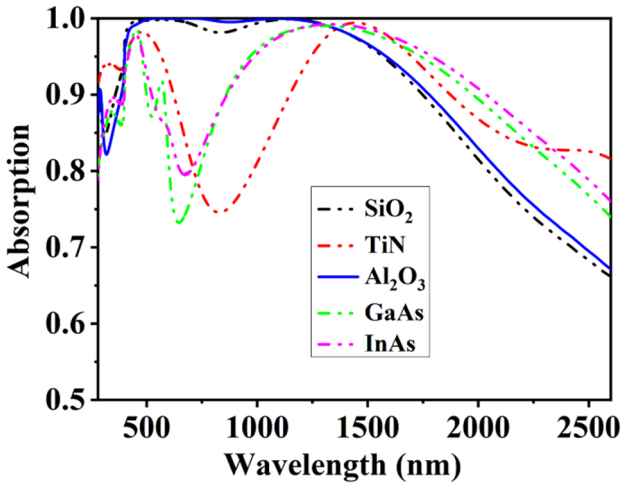

Figure 10. Absorption spectral of different dielectric materials.

Next, we investigated the detailed geometric parameters of the proposed arrays. By simulating the changes in different geometric parameters one by one, we finally determined the optimal parameters of arrays to obtain the best absorption effect. In the previous study, the absorption mechanism of the absorber was analyzed. The upper and bottom metal Ti and the middle dielectric constitute the LC circuit [48]. The periodic units can also be regarded as LC circuits. The increase in capacitance causes the red shift of the resonance peak but absorptivity is reduced. The formula of the resonance wavelength and inductance and capacitance refers to [49,50]:

$$\lambda \approx 2\pi c_0 \sqrt{(L_m + L_k)C_m} \quad (2)$$

In this formula, L_m is the parallel-plate inductance per unit length, L_k is the kinetic inductance and C_m is the parallel-plate capacitance.

First, we discussed the period P of the overall arrays. The results of the increasing period P from 380 nm to 420 nm in 10 nm steps are presented in Figure 11a. As the period P increases from 380 nm to 420 nm, the bandwidth of absorption above 90% decreases from 1518 nm to 1275 nm. The narrowing of the bandwidth increases the average absorptivity by 2% from 385 nm to 1150 nm where the solar radiation is more distributed. Therefore, finally, 400 nm was chosen as the period P, which can obtain ideal absorptivity. Subsequently, we discussed the influence of the radiuses R, r and a of the cross elliptical disks on the overall absorptivity, and the result is presented in Figure 11b–d. We can see that the absorption of the proposed absorber is insensitive with changes in the structural parameters at a short wavelength. The overall absorption bandwidth broadens out from 1086 nm to 1690 nm as R increases from 150 nm to 190 nm in steps of 10 nm. At the same time, although the wavelength at which the absorption intensity peak appears is red-shifted from 900 nm to 1350 nm, the peak decreases by 3.4% from 99.9% to 96.5%. Changes in r and R have similar influences. When r = 45 nm, there is only one absorption peak of 99.6% at 425 nm, and the absorption peak is red-shifted from 883 nm to 1528 nm, but the peak increased from 98.7% to 99.9% and then decreased to 99.4%. These results are caused by the increase in inductance and capacitance with the increase in geometric size. When r is longer than 65 nm, both perform well in the short wavelength and long wavelength band, but absorptivity is reduced by 4% at most between 700 nm and 1100 nm. For the widest possible absorption bandwidth and an excellent absorption effect, R = 170 nm and r = 65 nm were adopted. Earlier we explained the effect of the air hole in the middle Ti metal layer as shown in Figures 6 and 7. Then, we investigated the influence of the cavity size (radius a) on total absorptivity. Although it has the same trend as Figure 11b,c, it is the opposite to that of the radius a decrease in Figure 11d, as the absorption bandwidth becomes wider. When a changes from 50 nm to 90 nm (R = 170 nm, r = 65 nm), the absorption bandwidth above 90% becomes narrow from 1561 nm to 354 nm. Before a increases to 70 nm, although the bandwidth is wider, there is a significant trough where the absorptivity decreases from 99.5% to 94.7% at 855 nm. After a = 70 nm, without a significant increase in the overall absorptivity, the absorption bandwidth becomes narrower, and even at a = 90 nm, the absorption bandwidth above 90% is only found at 354 nm, as shown by the purple line in Figure 11d, which is unacceptable. We chose R = 170 nm, r = 65 nm and a = 70 nm as the ellipse parameters that make up the cross elliptical disk to obtain the best absorption effect. These changes have an impact on the excitation of the SPR effect [51,52]. When the energy around the arrays decreases, indicating that more energy is lost in the process, the light absorption becomes less effective.

As mentioned above, the proposed solar absorber is composed of four layers (Al_2O_3-Ti-Al_2O_3-Ti). In Figures 8 and 9, we investigate different stacking cases of Al_2O_3 and Ti to figure out that each part is necessary. Here, we further studied the effect of different thicknesses of the Al_2O_3 and Ti layers on absorption performance while keeping other parameters unchanged. We know that the key role in light absorption is the Al_2O_3 layer between the metals. The Al_2O_3 layer covering the top of the structure has little effect on absorptivity. Similarly, we can see in Figure 12a that the thickness of h_1 increases from 20 nm to 100 nm, and the emerged absorption bandwidth above 90% becomes narrow from 1485 nm to 1340 nm. Nevertheless, there is still h_1 = 60 nm, which has the highest average absorptivity of 99.6% at approximately 400 nm to 1150 nm where solar energy is more concentrated, as in our choice. In Figure 12b, the height of the Ti structure and air hole layer h_2 was changed to determine the effect it can have on absorption performance. It is different from Figure 12a: when h_2 increases from 95 nm to 135 nm in steps of 10 nm, the total absorption bandwidth becomes wider from 1170 nm to 1555 nm and the short wavelength region remains almost unchanged. However, a wider absorption bandwidth reduces absorptivity from 99.5% to 98.1%. Considering the distribution of solar energy in practical applications, we think it is more important to abandon a cer-

tain bandwidth to increase the absorption (almost 100%) in this area. The thickness of h_2 = 115 nm became our final choice for the proposed material. For the influence of the changes in h_3, it is similar but weaker when compared with the changes in h_2 on absorption (Figure 12c). Due to capacitation increases, when h_3 increases from 50 nm to 90 nm, the bandwidth of absorptivity above 90% becomes wider from 1245 nm to 1489 nm but absorptivity decreases from 99.5% to 98.2%. That is why we decided to use h_3 = 70 nm as the thickness of the Al_2O_3 layer between metals. The intensity change in the excited SPR is the physical reason for the effect of these parameters' change on light absorption performance. The increased thickness of these layers reduces the reflection of arrays and thus improves absorptivity, while an excessive thickness is also detrimental to SPR [53,54]. The proper thickness excites the resonance in the most effective way and obtains the best absorption performance.

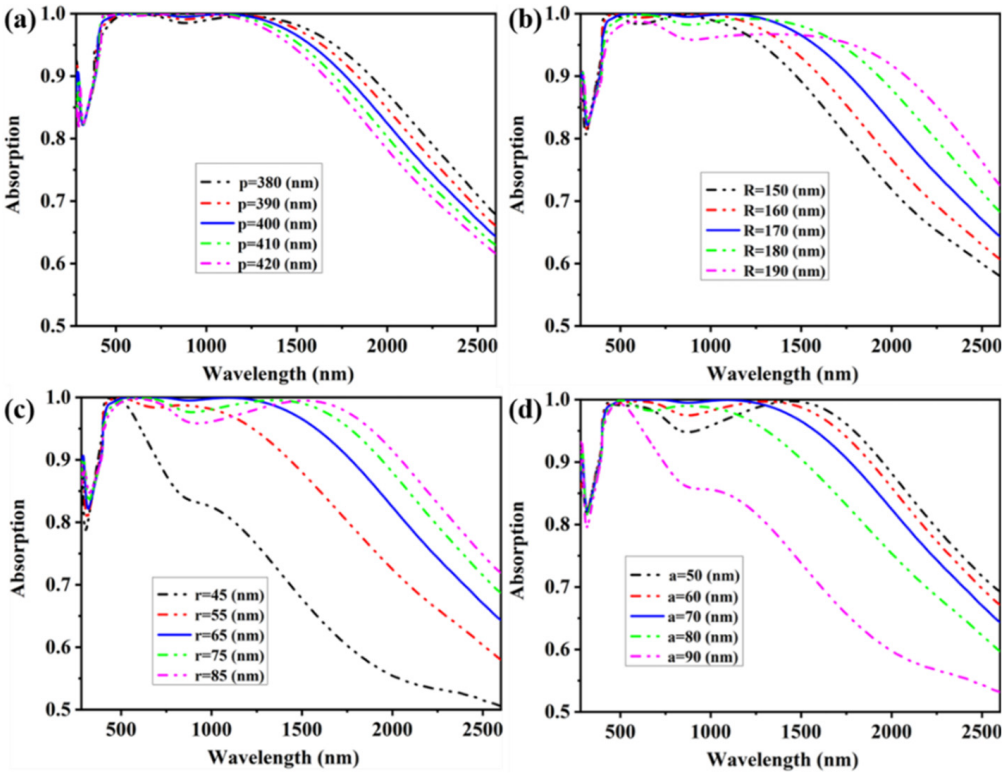

Figure 11. (**a**) Absorption spectrum at different periods. (**b**–**d**) The influence of the geometric parameters of the cross ellipse disks' nanostructure on the absorption.

The ideal solar absorber should be insensitive to the polarization angle and oblique incident angle [55,56]. As presented in Figure 13, we calculated the capability at different oblique incident angles from 0° to 60° under the TM mode and TE mode, respectively. In this calculation, we used the Case4 structure, and adopted the geometric parameters of the structure and design section. We found that our proposed absorber keeps an excellent absorptivity in a wide bandwidth. The total absorption bandwidth starts to narrow when the incident angle increases to nearly 60°. It indicates that the oblique incidence angle has little effect on overall absorption. It is obvious that the proposed material under the TE and TM modes performed the same. The high symmetry of the cross elliptical disk arrays contributes to the polarization independence of the absorber. The above analyzed results demonstrate that our proposed absorber still has good absorption ability for complex light in a real application [57–59].

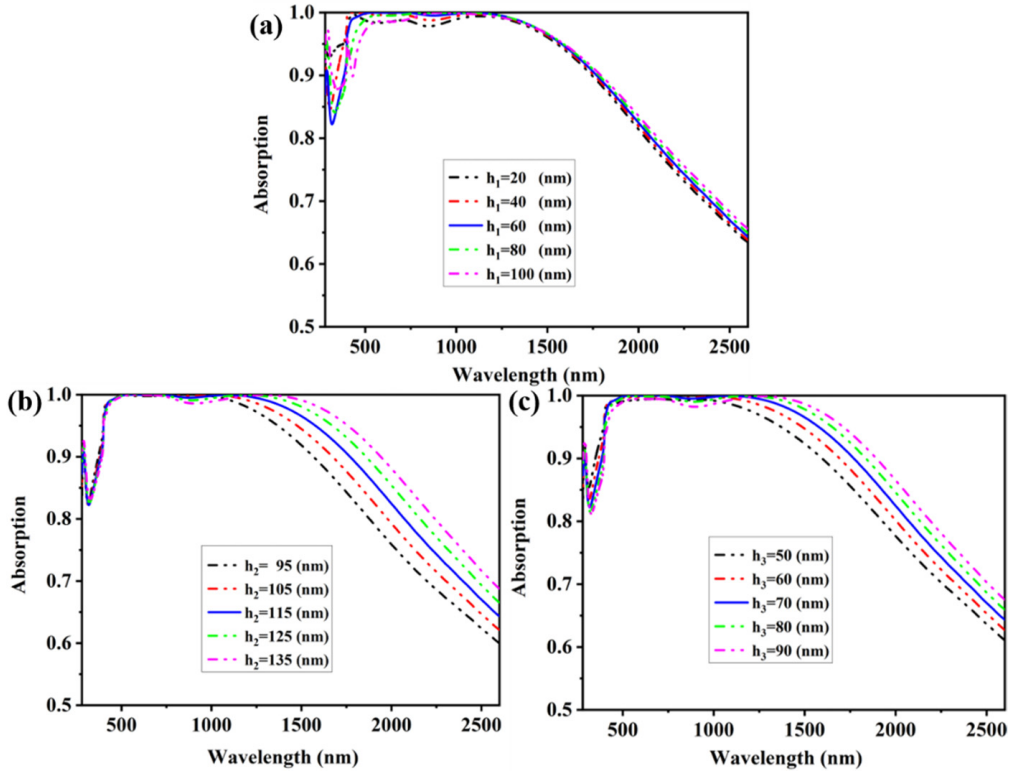

Figure 12. (**a**) The influence of the thicknesses of top Al_2O_3 layers on the absorption. (**b**) The influence of the thicknesses of mid metal Ti layers on the absorption. (**c**) The influence of the thicknesses of middle Al_2O_3 layers on the absorption.

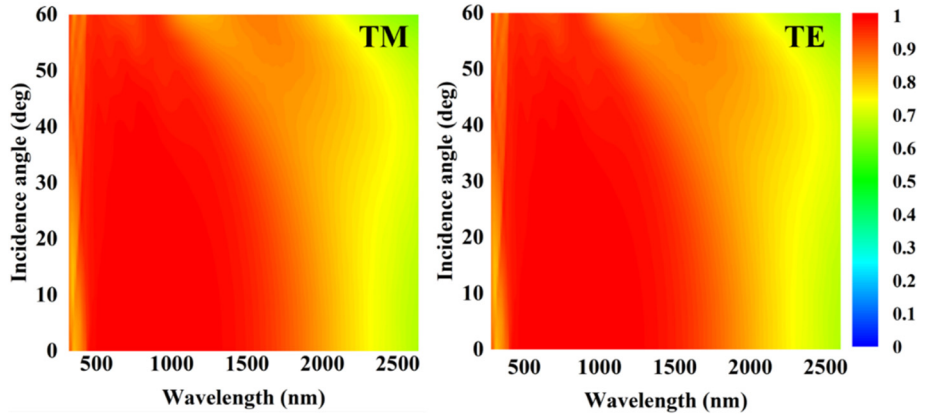

Figure 13. Absorption spectra of oblique incident angle for TM and TE modes, respectively.

4. Conclusions

In this paper, we proposed a metamaterial solar absorber with a cross elliptical disk structure. The structure can excite strong surface plasmon resonance, and the addition of a cavity in the structure greatly improves the absorption of 500–1326 nm. Therefore, the proposed absorber achieves 98.78% high absorption performance in the broadband operating range of 385–1765 nm. It is perfectly matched with the solar radiation band, with only a 1.6% loss in the 280–2600 nm, which is the actual existing solar radiation. In addition, the proposed absorber is insensitive to angle changes and independent of polarization, and the thickness is only 445 nm. In future work, we will focus on optimizing the structure and reducing the difficulty of its fabrication so that it can be prepared s part of an experiment. In summary, the proposed absorber is very thin and composed of high-temperature resistant materials. Polarization insensitivity and large angle incident

absorption makes it have potential application value in a wide range of solar energy utilization fields such as thermophotovoltaics, solar energy harvesting and shielding.

Author Contributions: Y.Z.: Conceptualization, formal analysis, investigation, data curation, writing—original draft, writing—review and editing. Y.Y. (Yingting Yi): Conceptualization, formal analysis, investigation, data curation, funding acquisition. W.L.: Conceptualization, formal analysis, investigation, data curation, writing—original draft, writing—review and editing. S.L.: Conceptualization, formal analysis, investigation, data curation, writing—original draft, writing—review and editing. J.M.: Conceptualization, formal analysis, investigation. S.C.: Conceptualization, formal analysis, investigation, data curation. W.Y.: Conceptualization, formal analysis, investigation. Y.Y. (Yougen Yi): Conceptualization, formal analysis, investigation. All authors have read and agreed to the published version of the manuscript.

Funding: The authors are grateful to the support by National Natural Science Foundation of China (No. 11774054, 12075036).

Institutional Review Board Statement: Not applicable.

Informed Consent Statement: Not applicable.

Data Availability Statement: Publicly available datasets were analyzed in this study. These data can be found here: [https://www.lumerical.com/] (accessed on 1 January 2020).

Conflicts of Interest: The authors declare no conflict of interest.

References

1. Hosseini, S.E.; Wahid, M.A. Hydrogen from solar energy, a clean energy carrier from a sustainable source of energy. *Int. J. Energy Res.* **2020**, *44*, 4110–4131. [CrossRef]
2. Kenisarin, M.; Mahkamov, K. Solar energy storage using phase change materials. *Renew. Sustain. Energy Rev.* **2007**, *11*, 1913–1965. [CrossRef]
3. Zhu, H.; Yi, F.; Cubukcu, E. Plasmonic metamaterial absorber for broadband manipulation of mechanical resonances. *Nat. Photonics* **2016**, *10*, 709–714. [CrossRef]
4. Yu, P.; Lucas, V.B.; Huang, Y.J.; Wu, J.; Fu, L.; Tan, H.H.; Jagadish, C.; Wiederrecht, G.P.; Govorov, A.O.; Wang, Z. Broadband metamaterial absorbers. *Adv. Opt. Mater.* **2019**, *7*, 1800995. [CrossRef]
5. Paracchino, A.; Brauer, J.C.; Moser, J.E.; Thimsen, E.; Graetzel, M. Synthesis and characterization of high-photoactivity electrodeposited Cu_2O solar absorber by photoelectrochemistry and ultrafast spectroscopy. *J. Phys. Chem. C* **2012**, *116*, 7341–7350. [CrossRef]
6. Zhou, Z.Y.; Liu, W.F.; Guo, Y.; Huang, H.L.; Ding, X.L. Design Simulation and Optimization of Germanium-Based Solar Cells with Micro-Nano Cross-Cone Absorption Structure. *Coatings* **2022**, *12*, 1653. [CrossRef]
7. Chen, H.; Chen, Z.; Yang, H.; Wen, L.; Yi, Z.; Zhou, Z.; Dai, B.; Zhang, J.; Wu, X.; Wu, P. Multi-mode surface plasmon resonance absorber based on dart-type single-layer graphene. *RSC Adv.* **2022**, *12*, 7821–7829. [CrossRef]
8. Agarwal, S.; Prajapati, Y.K. Design of broadband absorber using 2-D materials for thermo-photovoltaic cell application. *Opt. Commun.* **2018**, *413*, 39–43. [CrossRef]
9. Wang, X.Y.; Lin, J.C.; Yan, Z.Y.; Yi, Z.; Yu, J.X.; Zhang, W.; Qin, F.; Wu, X.W.; Zhang, J.G.; Wu, P.H. Tunable high-sensitivity sensing detector based Bulk Dirac semimetal. *RSC Adv.* **2022**, *12*, 32583. [CrossRef]
10. Zheng, Z.; Zheng, Y.; Luo, Y.; Yi, Z.; Zhang, J.; Liu, Z.; Yang, W.; Yu, Y.; Wu, X.; Wu, P. A switchable terahertz device combining ultra-wideband absorption and ultra-wideband complete reflection. *Phys. Chem. Chem. Phys.* **2022**, *24*, 2527–2533. [CrossRef]
11. Ng, C.; Yap, L.W.; Roberts, A.; Cheng, W.; Gómez, D.E. Black gold: Broadband, high absorption of visible light for photochemical systems. *Adv. Funct. Mater.* **2017**, *27*, 1604080. [CrossRef]
12. Yi, Z.; Li, J.K.; Lin, J.C.; Qin, F.; Chen, X.F.; Yao, W.T.; Liu, Z.M.; Cheng, S.B.; Wu, P.H.; Li, H.L. Broadband polariza-tion-insensitive and wide-angle solar energy absorber based on tungsten ring-disc array. *Nanoscale* **2020**, *12*, 23077–23083. [CrossRef] [PubMed]
13. Yu, P.; Yang, H.; Chen, X.; Yi, Z.; Yao, W.; Chen, J.; Yi, Y.; Wu, P. Ultra-wideband solar absorber based on refractory titanium metal. *Renew. Energy* **2020**, *158*, 227–235. [CrossRef]
14. Li, J.K.; Chen, X.F.; Yi, Z.; Yang, H.; Tang, Y.J.; Yi, Y.; Yao, W.T.; Wang, J.Q.; Yi, Y.G. Broadband solar energy absorber based on monolayer molybdenum disulfide using tungsten elliptical arrays. *Mater. Today Energy* **2020**, *16*, 100390. [CrossRef]
15. Nguyen, T.T.; Lim, S. Angle-and polarization-insensitive broadband metamaterial absorber using resistive fan-shaped resonators. *Appl. Phys. Lett.* **2018**, *112*, 021605. [CrossRef]
16. Landy, N.I.; Sajuyigbe, S.; Mock, J.J.; Smith, D.R.; Padilla, W.J. Perfect metamaterial absorber. *Phys. Rev. Lett.* **2008**, *100*, 207402. [CrossRef]

17. Zhao, F.; Lin, J.; Lei, Z.; Yi, Z.; Qin, F.; Zhang, J.; Liu, L.; Wu, X.; Yang, W.; Wu, P. Realization of 18.97% theoretical efficiency of 0.9 μm thick c-Si/ZnO heterojunction ultrathin-film solar cells via surface plasmon resonance enhancement. *Phys. Chem. Chem. Phys.* **2022**, *24*, 4871–4880. [CrossRef]
18. Zhang, C.; Yi, Y.; Yang, H.; Yi, Z.; Chen, X.; Zhou, Z.; Yi, Y.; Li, H.; Chen, J.; Liu, C. Wide spectrum solar energy absorption based on germanium plated ZnO nanorod arrays: Energy band regulation, Finite element simulation, Super hydrophilicity, Photothermal conversion. *Appl. Mater. Today* **2022**, *28*, 101531. [CrossRef]
19. Haegglund, C.; Zeltzer, G.; Ruiz, R.; Wangperawong, A.; Roelofs, K.E.; Bent, S.F. Strong coupling of plasmon and nanocavity modes for dual-band, near-perfect absorbers and ultrathin photovoltaics. *ACS Photonics* **2016**, *3*, 456–463. [CrossRef]
20. Lee, D.; Jeong, H.; Lim, S. Electronically switchable broadband metamaterial absorber. *Sci. Rep.* **2017**, *7*, 4891. [CrossRef]
21. Wang, H.C.; Chen, Q.; Wen, L.; Song, S.; Hu, X.; Xu, G. Titanium-nitride-based integrated plasmonic absorber/emitter for solar thermophotovoltaic application. *Photonics Res.* **2015**, *3*, 329–334. [CrossRef]
22. Guler, U.; Ndukaife, J.C.; Naik, G.V. Local heating with lithographically fabricated Plasmonic titanium nitride nanoparticles. *Nano Lett.* **2013**, *13*, 6078–6083. [CrossRef] [PubMed]
23. Hu, C.; Liu, L.; Zhao, Z.; Chen, X.; Luo, X. Mixed plasmons coupling for expanding the bandwidth of near-perfect absorption at visible frequencies. *Opt. Express* **2009**, *17*, 16745–16749. [CrossRef] [PubMed]
24. Cui, Y.; Fung, K.H.; Xu, J.; Ma, H.; Jin, Y.; He, S.; Fang, N.X. Ultrabroadband light absorption by a sawtooth anisotropic metamaterial slab. *Nano Lett.* **2012**, *12*, 1443–1447. [CrossRef] [PubMed]
25. Chen, M.; He, Y. Plasmonic nanostructures for broadband solar absorption based on the intrinsic absorption of metals. *Sol. Energy Mater. Sol. Cells* **2018**, *188*, 156–163. [CrossRef]
26. Chen, Y. Nanofabrication by electron beam lithography and its applications. *Microelectron. Eng.* **2015**, *135*, 57–72. [CrossRef]
27. Ding, F.; Mo, L.; Zhu, J.; He, S. Lithography-free, broadband, omnidirectional, and polarization-insensitive thin optical absorber. *Appl. Phys. Lett.* **2015**, *106*, OP98–OP953. [CrossRef]
28. Zhou, Y.; Qin, Z.; Liang, Z.; Meng, D.; Xu, H.; Smith, D.R.; Liu, Y. Ultra-broadband metamaterial absorbers from long to very long infrared regime. *Light-Sci. Appl.* **2021**, *10*, 138. [CrossRef]
29. Deng, Y.; Cao, G.; Yang, H.; Zhou, X.; Wu, Y. Dynamic Control of Double Plasmon-Induced Transparencies in Aperture-Coupled Waveguide-Cavity System. *Plasmonics* **2018**, *13*, 345–352. [CrossRef]
30. Shangguan, Q.Y.; Chen, Z.H.; Yang, H.; Cheng, S.B.; Yang, W.X.; Yi, Z.; Wu, X.W.; Wang, S.F.; Yi, Y.G.; Wu, P.H. Design of Ultra-Narrow Band Graphene Refractive Index Sensor. *Sensors* **2022**, *22*, 6483. [CrossRef]
31. Edward, D.P.; Palik, I. *Handbook of Optical Constants of Solids*; Academic Press: New York, NY, USA, 1985.
32. Gu, Y.F.; Guo, B.B.; Yi, Z.; Wu, X.W.; Zhang, J.; Yang, H. Morphology modulation of hollow-shell $ZnSn(OH)_6$ for enhanced photodegradation of methylene blue. *Colloids Surfaces A Physicochem. Eng. Asp.* **2022**, *653*, 129908. [CrossRef]
33. Li, L.; Gao, H.; Liu, G.; Wang, S.; Yi, Z.; Wu, X.; Yang, H. Synthesis of carnation flower-like $Bi_2O_2CO_3$ photocatalyst and its promising application for photoreduction of Cr(VI). *Adv. Powder Technol.* **2022**, *33*, 103481. [CrossRef]
34. Liu, Y.; Bo, M.; Yang, X.; Zhang, P.; Sun, C.Q.; Huang, Y. Size modulation electronic and optical properties of phosphorene nanoribbons: DFT–BOLS approximation. *Phys. Chem. Chem. Phys.* **2017**, *19*, 5304–5309. [CrossRef] [PubMed]
35. Tang, P.; Liu, G.; Liu, X.; Fu, G.; Liu, Z.; Wang, J. Polasmonic wavy surface for ultrathin semiconductor black absorbers. *Opt. Express* **2020**, *28*, 27764–27773. [CrossRef] [PubMed]
36. Li, J.; Chen, Z.; Yang, H.; Yi, Z.; Chen, X.; Yao, W.; Duan, T.; Wu, P.; Li, G.; Yi, Y. Tunable broadband solar energy absorber based on monolayer transition metal dichalcogenides materials using Au nanocubes. *Nanomaterials* **2020**, *10*, 257. [CrossRef]
37. Akafzade, H.; Sharma, S.C. New metamaterial as a broadband absorber of sunlight with extremely high absorption efficiency. *AIP Adv.* **2020**, *10*, 1063. [CrossRef]
38. Liu, F.; Qi, L. A simple two-layer broadband metamaterial absorber for solar cells. *Mod. Phys. Lett. B* **2021**, *17*, 2150291. [CrossRef]
39. Zhong, H.; Liu, Z.; Tang, P.; Liu, X.; Zhan, X.; Pan, P.; Tang, C. Thermal-stability resonators for visible light full-spectrum perfect absorbers. *Sol. Energy* **2020**, *208*, 445–450. [CrossRef]
40. Agarwal, S.; Srivastava, G.; Prajapati, Y.K. Dual Band Vis-IR Absorber Using Bismuth Based Helical Metamaterial Surface. *Opt. Quant. Electron.* **2022**, *54*, 772. [CrossRef]
41. Qin, F.; Chen, X.; Yi, Z.; Yao, W.; Yang, H.; Tang, Y.; Yi, Y.; Li, H.; Yi, Y. Ultra-broadband and wide-angle perfect solar absorber based on TiN nanodisk and Ti thin film structure. *Sol. Energy Mater. Sol. Cells* **2020**, *211*, 110535. [CrossRef]
42. Li, L.; Gao, H.; Yi, Z.; Wang, S.; Wu, X.; Li, R.; Yang, H. Comparative investigation on synthesis, morphological tailoring and photocatalytic activities of $Bi_2O_2CO_3$ nanostructures. *Colloids Surfaces A Physicochem. Eng. Asp.* **2022**, *644*, 128758. [CrossRef]
43. Cai, L.; Zhang, Z.; Xiao, H.; Chen, S.; Fu, J. An eco-friendly imprinted polymer based on graphene quantum dots for fluorescent detection of *p*-nitroaniline. *RSC Adv.* **2019**, *9*, 41383–41391. [CrossRef] [PubMed]
44. Zhu, W.L.; Yi, Y.T.; Yi, Z.; Bian, L.; Yang, H.; Zhang, J.G.; Yu, Y.; Liu, C.; Li, G.F.; Wu, X.W. High confidence plasmonic sensor based on photonic crystal fiber with U-shaped detection channel. *Phys. Chem. Chem. Phys.* **2023**. [CrossRef]
45. Shangguan, Q.Y.; Chen, H.; Yang, H.; Liang, S.R.; Zhang, Y.J.; Cheng, S.B.; Yang, W.X.; Yi, Z.; Luo, Y.; Wu, P.H. A "belfry-typed" narrow-band tunable perfect absorber based on graphene and the application potential research. *Diam. Relat. Mater.* **2022**, *125*, 108973. [CrossRef]
46. Zheng, Z.; Luo, Y.; Yang, H.; Yi, Z.; Zhang, J.; Song, Q.; Yang, W.; Liu, C.; Wu, X.; Wu, P. Thermal tuning of terahertz metamaterial properties based on phase change material vanadium dioxide. *Phys. Chem. Chem. Phys.* **2022**, *24*, 8846–8853. [CrossRef]

47. Feng, R.; Liu, J.; Liu, L.H.; Ding, W.; Chen, L. Parallel LC circuit model for multiband absorption and preliminary design of radiative cooling. *Opt. Express* **2014**, *22*, 1713–1724. [CrossRef]
48. Zhou, Z.; Chen, Y.; Tian, Y.; Liang, J.; Yang, W. Ultra-broadband metamaterial perfect solar absorber with polarization-independent and large incident angle-insensitive. *Opt. Laser Technol.* **2022**, *156*, 108591. [CrossRef]
49. Lv, P.; Xie, D.; Zhang, Z. Magnetic carbon dots based molecularly imprinted polymers for fluorescent detection of bovine hemoglobin. *Talanta* **2018**, *188*, 145–151. [CrossRef]
50. Shangguan, Q.Y.; Zhao, Y.; Song, Z.J.; Wang, J.; Yang, H.; Chen, J.; Liu, C.; Cheng, S.B.; Yang, W.X.; Yi, Z. High sensitivity active adjustable graphene absorber for refractive index sensing applications. *Diam. Relat. Mater.* **2022**, *128*, 109273. [CrossRef]
51. Zhou, F.; Qin, F.; Yi, Z.; Yao, W.-T.; Liu, Z.; Wu, X.; Wu, P. Ultra-wideband and wide-angle perfect solar energy absorber based on Ti nanorings surface plasmon resonance. *Phys. Chem. Chem. Phys.* **2021**, *23*, 17041–17048. [CrossRef]
52. Liang, S.R.; Xu, F.; Yang, H.; Cheng, S.B.; Yang, W.X.; Yi, Z.; Song, Q.J.; Wu, P.H.; Chen, J.; Tang, C.J. Ultra long infrared metamaterial absorber with high absorption and broad band based on nano cross surrounding. *Opt. Laser Technol.* **2023**, *158*, 108789. [CrossRef]
53. Wang, D.Y.; Yi, Z.; Ma, G.L.; Dai, B.; Yang, J.B.; Zhang, J.F.; Yu, Y.; Liu, C.; Wu, X.W.; Bian, Q. Two channels photonic crystal fiber based on surface plasmon resonance for magnetic field and temperature dual-parameter sensing. *Phys. Chem. Chem. Phys.* **2022**, *24*, 21233. [CrossRef] [PubMed]
54. Luo, W.H.; Cao, W.X.; Bruijnincx, P.C.A.; Lin, L.; Wang, A.Q.; Zhang, T. Zeolite-supported metal catalysts for selective hydrodeoxygenation of biomass-derived platform molecules. *Green Chem.* **2019**, *21*, 3744–3768. [CrossRef]
55. Wu, X.; Zheng, Y.; Luo, Y.; Zhang, J.; Yi, Z.; Wu, X.; Cheng, S.; Yang, W.; Yu, Y.; Wu, P. A four-band and polarization-independent BDS-based tunable absorber with high refractive index sensitivity. *Phys. Chem. Chem. Phys.* **2021**, *23*, 26864–26873. [CrossRef]
56. Zhao, F.; Chen, X.F.; Yi, Z.; Qin, F.; Tang, Y.J.; Yao, W.T.; Zhou, Z.G.; Yi, Y.G. Study on the solar energy absorption of hybrid solar cells with trapezoid-pyramidal structure based PEDOT:PSS/c-Ge. *Solar Energy* **2020**, *204*, 635–643. [CrossRef]
57. Lin, X.; Li, Y.J.; Chen, F.T.; Xu, P.; Li, M. Facile synthesis of mesoporous titanium dioxide doped by Ag-coated graphene with enhanced visible-light photocatalytic performance for methylene blue degradation. *RSC Adv.* **2017**, *7*, 25314–25324. [CrossRef]
58. Su, J.; Yang, H.; Xu, Y.; Tang, Y.J.; Yi, Z.; Zheng, F.S.; Zhao, F.; Liu, L.; Wu, P.H.; Li, H.L. Based on Ultrathin PEDOT:PSS/c-Ge Solar Cells Design and Their Photoelectric Performance. *Coatings* **2021**, *11*, 748. [CrossRef]
59. Li, Y.; Liu, Z.; Zhang, H.; Tang, P.; Wu, B.; Liu, G. Ultra-broadband perfect absorber utilizing refractory materials in metal-insulator composite multilayer stacks. *Opt. Express* **2019**, *27*, 11809–11818. [CrossRef]

Disclaimer/Publisher's Note: The statements, opinions and data contained in all publications are solely those of the individual author(s) and contributor(s) and not of MDPI and/or the editor(s). MDPI and/or the editor(s) disclaim responsibility for any injury to people or property resulting from any ideas, methods, instructions or products referred to in the content.